Inorganic Chemistry

Article

pubs.acs.org/IC

$AgNb_7O_{18}$: An Ergodic Relaxor Ferroelectric

David I. Woodward* and Richard Beanland

Department of Physics, University of Warwick, Gibbet Hill Road, Coventry, CV4 7AL, U.K.

Supporting Information

ABSTRACT: $AgNb_7O_{18}$ is a relaxor ferroelectric with a Burns temperature of ~490 K and an incipient transition to the nonergodic state. The short-range structure is shown by convergent-beam electron diffraction to have the polar space group *Im*2*m*, but refinements against powder X-ray diffraction find the long-range structure to have the centrosymmetric space group *Immm*. Relaxor behavior in $AgNb_7O_{18}$ appears to originate from the partial occupation of large interstices by Ag^+ cations. Both cations and oxygen anions are displaced away from zones where NbO_6 octahedra are edge-sharing.

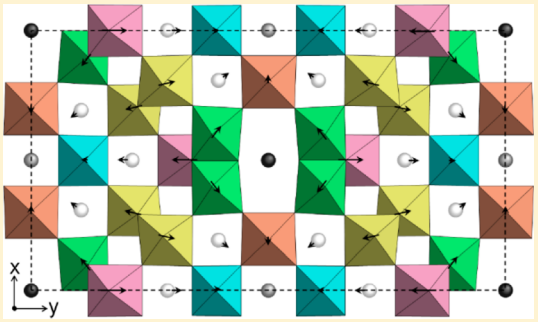

INTRODUCTION

Ferroelectric ceramics are used in an enormous variety of technological applications, and the majority of these materials are based on the perovskite structure. This is for well-established reasons: the prototype structure is simple and particularly flexible, allowing it to accommodate most cations and thus access a wide range of properties which can then be "tuned" to specific applications by control of the ionic content.[1] The research into perovskite-structured materials has developed rapidly but at the price of a lack of research into other ferroelectric structures. The continued development of functional materials and devices requires the identification of crystal structures above and beyond perovskites that can be used to host physical properties and be structurally tuned for specific applications as diverse as temperature-independent dielectrics,[2] thermoelectrics,[3] and multiferroics.[4]

The $Ag_2O-Nb_2O_5$ pseudobinary system is known to host an unusually large number of distinct crystal structures[5] with five confirmed structures and a number of additional, unconfirmed structures. Among the former are the perovskite-structured ferrielectric $AgNbO_3$,[6] the ferroelectric $Ag_2Nb_4O_{11}$,[7] which has the layered natrotantite structure containing edge-shared NbO_7 polyhedra,[8] and the tungsten bronze-structured $AgNb_3O_8$.[9] The system is rich with functional materials: $AgNbO_3$ is a compound studied for its role in lead-free piezoelectrics,[10] reentrant relaxors,[11] and photocatalysis.[12] $Ag_2Nb_4O_{11}$-structured materials are finding value in the study of tunable band gap materials for photocatalyzing the electrolysis of water[13] and in investigations of the anomalously large piezoelectric coefficients of Ta_2O_5 thin films.[14,15] Tungsten bronzes are studied for their ferroelectric properties[16] and for their potential use in thermoelectric applications.[17]

However, $AgNb_7O_{18}$ and $AgNb_{13}O_{33}$ are compounds about which little is currently known, although structural studies of the sodium analogues have been performed. The structure of $NaNb_7O_{18}$ was studied and refined by Marinder and Sundberg,[18] who found that the positions of diffraction peaks were consistent with an orthorhombic body-centered unit cell. The systematic absences limited the choice to four possible space groups: *I*222, $I2_12_12_1$, *Imm*2, and *Immm*. The authors chose *Immm*, but without an explanation for rejecting the other space groups. Of the four symmetries, *Immm* is the only centrosymmetric option and precludes the existence of functional properties such as piezoelectricity or ferroelectricity.

The crystal structure of $NaNb_7O_{18}$ consists of units formed from 14 corner-sharing NbO_6 octahedra in a perovskite-like arrangement. These units are linked together by edge-sharing of the octahedra at the perimeters, resulting in the appearance of tunnels with a large rectangular cross section. Marinder and Sundberg[18] proposed that half of the Na^+ ions would be located in these tunnels, and the remainder would be distributed in the cuboctahedral interstices within the perovskite-like units. They recommended studying $AgNb_7O_{18}$ as the larger Ag^+ ions would be easier to locate using diffraction methods. A recent study[9] fabricated crystals of $AgNb_7O_{18}$ and showed that the crystal structure is isostructural with that of $NaNb_7O_{18}$, but no refined structures exist for $AgNb_7O_{18}$ and its physical properties are not known.

Nb^{5+} appears in a significant proportion of ferroelectric oxides[3] in octahedral coordination where it has a tendency to displace off-center.[19,20] If these Nb^{5+} displacements in the unit cell are correlated with a common component, the material becomes polarized. If the common component can be switched by an external field, the material is ferroelectric. The construction of $AgNb_7O_{18}$ from perovskite-like units makes it particularly likely to exhibit ferroelectricity. To investigate this possibility, ceramics have been synthesized and the structure and dielectric properties investigated.

Received: March 31, 2014
Published: August 12, 2014

   dx.doi.org/10.1021/ic5007346 | *Inorg. Chem.* 2014, 53, 8941−8948

EXPERIMENTAL METHODS

$AgNb_7O_{18}$ was synthesized by a conventional solid state processing route. Ag_2O (Alfa Aesar, 99%) and Nb_2O_5 (Alfa Aesar, 99%) were weighed out in stoichiometric amounts and ball-milled with 1 cm zirconia media in propan-2-ol for approximately 24 h. This mixture was dried at 70 °C and passed through a 250 μm sieve before being reacted for 10 h at 1050 °C. The reacted material was remilled for a further 24 h, before being dried and sieved as before. This resulted in a fine powder, which was compacted into 13 mm diameter pellets using a load of 1 ton. These pellets were buried in a bed of $AgNb_7O_{18}$ powder in an alumina crucible and sintered for 2 h at 1250 °C. Ceramic densities were calculated from measurements of pellet dimensions and masses.

Dielectric measurements were performed using an HP 4192A LF impedance analyzer. Electrodes were applied to ceramics using silver paint (RS Components), and the ceramics were cooled with liquid nitrogen at a rate of approximately 0.5 °C min^{-1} during data collection. High-temperature data were obtained with a rig located in a vertical tube furnace using a heating rate of 1 °C min^{-1} during data collection. A layer of sputtered gold was added before the silver paint to prevent the silver from reacting with the ceramic at high temperatures.

Transmission electron microscopy (TEM) was performed on a JEOL JEM-2100 electron microscope at 200 kV. $AgNb_7O_{18}$ pellets were thinned to ~30 μm with abrasive paper and perforated with a Gatan PIPS ion mill before being carbon-coated. Digital large-angle convergent beam electron diffraction (D-LACBED) patterns were obtained using recently developed code made freely available.[21] Crystal simulations were performed using CaRine Crystallography v3.1, and electron diffraction simulations were performed using SingleCrystal v2.2.8.

Powder samples were prepared for X-ray diffraction (XRD) by grinding pellets in acetone with a pestle and mortar. XRD was performed using a Panalytical X'Pert Pro with a curved Ge Johansson monochromator excluding all X-rays except Cu $K\alpha_1$. The scan was performed at 40 kV and 45 mA from 6 to 120° 2θ with a step size of 0.066° 2θ over a period of 17 h and with a Panalytical PIXcel detector. Rietveld refinements were performed with Topas Academic v4.1.

RESULTS AND DISCUSSION

Permittivity. Ceramic pellets were found to have a mean density of 4.62 (4) g cm^{-3}. Using the lattice parameters published by Rozier and Szajwaj[9] and assuming no Ag loss, this translates to pellets with densities that are 95.6 (7)% of the theoretical maximum, as defined by the unit cell density.

A structure formed from perovskite-like columns is likely to exhibit displacive phase transitions or functional properties. Dielectric permittivity data can indicate the presence of phase transitions and were collected for $AgNb_7O_{18}$ (Figure 1).

The relative permittivity, ε_r, takes fairly modest values similar to those observed for $Ag_2Nb_4O_{11}$.[22] However, the resistivity of $AgNb_7O_{18}$ is 30–40 MΩ·m recorded at 295 K and 1 kHz. These are surprisingly high values, given the presence of rectangular tunnels that might be expected to allow Ag^+ to travel with relative ease through the crystal structure.

The permittivity data in Figure 1 show a broad, frequency-dependent peak: behavior characteristic of a relaxor ferroelectric.[23] A relaxor is a material that, like a classical ferroelectric, possesses an electric dipole, but the dipoles do not have long-range order. Instead, the structure is thought to consist of nanoscale clusters of parallel dipoles, called "polar nanoregions" (PNRs), with a size distribution that results in the frequency distribution observed in Figure 1. Below the Burns temperature, T_B, the material is in the "ergodic" state, where these dipoles are fluctuating.[24] At lower temperatures, in the "nonergodic" state, the dipoles are frozen and an external field

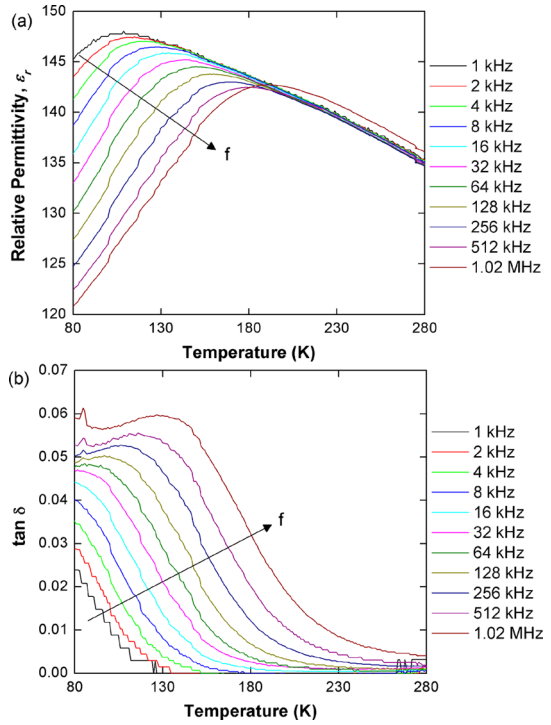

Figure 1. (a) Dielectric permittivity and (b) loss tangent for $AgNb_7O_{18}$ obtained across a range of frequencies at low temperature. The arrow marked "f" indicates the effect of increasing frequency.

can be used to pole the material and make it behave as a classical ferroelectric.[25]

The Vogel–Fulcher model was originally used to describe the magnetic relaxation in spin-glass systems but has been shown to be applicable to relaxor materials in describing the temperature of permittivity maximum as a function of frequency.[24] The model is

$$f = f_0 \exp[-E_a/k(T_m - T_F)] \quad (1)$$

where f_0 is the "Debye frequency", the theoretical maximum frequency for the vibration of PNRs, E_a is an activation energy, k is the Boltzmann constant, T_m is the temperature of the permittivity maximum at frequency f, and T_F is the freezing temperature that indicates the transition between the ergodic and nonergodic states. By plotting $\ln(f)$ as a function of temperature (Figure 2), the Vogel–Fulcher model can be fitted to the data by a least-squares method and the material parameters can be derived.

Fitting the Vogel–Fulcher model to the permittivity data gives the following parameters with 95% confidence bounds:

$$T_F = -81 \text{ K } (-122, -39)$$

$$f_0 = 6.5 \times 10^{12} \text{ Hz } (2.4 \times 10^{11}, 1.8 \times 10^{14})$$

$$E_a = 0.37 \text{ eV } (0.23, 0.50)$$

These parameters are useful in comparing the relaxation properties of this material with those of more common relaxors, such as tungsten bronze or perovskite-structured relaxors. It should be noted that the Vogel–Fulcher relationship applied to the maxima in permittivity with temperature may yield values of the parameters that have some dependency on temperature and frequency.[26] The parameters derived from the permittivity data

dx.doi.org/10.1021/ic5007346 | Inorg. Chem. 2014, 53, 8941–8948

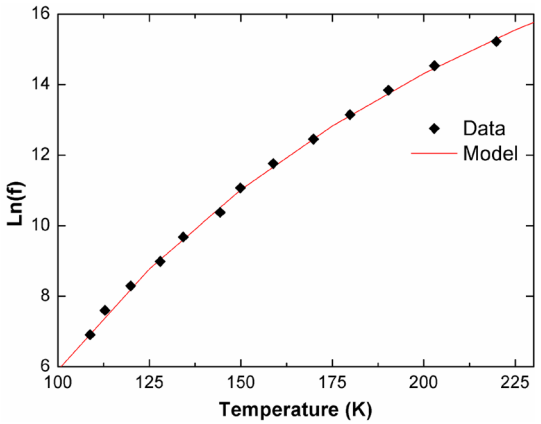

Figure 2. Log of frequency as a function of the temperature of permittivity maximum encountered on cooling for $AgNb_7O_{18}$. Data obtained from Figure 1a are plotted, along with the Vogel–Fulcher model fitted to these data.

are therefore accompanied by 95% confidence bounds to indicate a range of error from using this analysis.

The values of f_0 and E_a are found to be similar in magnitude to materials based on $Sr_4Nd_2Ti_4Nb_6O_{30}$, a tungsten bronze structured relaxor.[27] The relatively large value of E_a obtained here indicates that the polarization fluctuation of a PNR requires more energy than in these tungsten bronzes and in many perovskite-structured relaxors and is therefore slower.[24] The parameter T_F of the Vogel–Fulcher model indicates the temperature below which all PNRs are frozen, allowing the material to be poled with an external field and made to behave in a manner similar to classical ferroelectrics.[25] The fit yields a negative value of T_F which appears to indicate that some PNRs will continue to fluctuate at absolute zero. Some dielectrics exhibit increasing permittivity on cooling that can be extrapolated to a Curie temperature below 0 K. These are "incipient ferroelectrics" (e.g., $Na_{1/2}Bi_{1/2}Cu_3Ti_4O_{12}$[28]), so it is proposed that the negative value of T_F indicates that $AgNb_7O_{18}$ has an incipient transition to the nonergodic state.

It is anticipated that isovalent ions such as K^+, Na^+, Li^+, and Cu^+ can be substituted into $AgNb_7O_{18}$ without a change in morphology.[29] Substitutions may freeze-in the dipoles and create a ferroelectric phase, as observed in $(Sr_xBa_{1-x})_4Nd_2Ti_4Nb_6O_{30}$ tungsten bronzes.[27] It has also been shown that ferroelectricity can be induced in tungsten bronzes by reducing the size of cations on specific sites.[16] If the role of the Ag^+ cation is to make this particular connectivity of the NbO_6 framework energetically favorable, it should also be possible to substitute for half the number of divalent cations of similar size, such as Ca^{2+} or Ba^{2+}. If substitutions result in T_F increasing to a value above 0 K, the nonergodic state becomes accessible and an applied electric field on cooling can create a field-induced ferroelectric state.

While T_F indicates the lowest temperature in which a relaxor is in an ergodic state, the upper temperature is indicated by T_B, often a few hundred degrees above T_F.[30] This can be experimentally determined by birefringence[31] but can also be obtained from the permittivity data over a temperature range above that where the dispersion is observed. According to the Curie–Weiss law,[32] above T_B, the susceptibility, χ, is related to ε_r by the equation

$$\chi = 1/(\varepsilon_r - 1) \quad (2)$$

but below T_B, the permittivity deviates from this relationship. For $AgNb_7O_{18}$, the temperature range 300–550 K is sufficiently far above the region of dispersion to obtain a value of T_B (Figure 3).

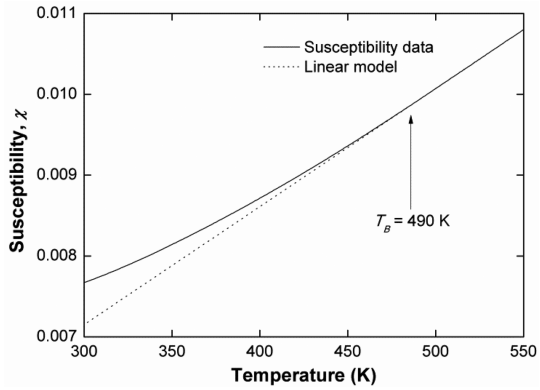

Figure 3. Susceptibility data for $AgNb_7O_{18}$ obtained at 1 MHz.

Figure 3 shows that T_B = 490 (10) K, indicating that $AgNb_7O_{18}$ is an ergodic relaxor ferroelectric at room temperature. Stringer et al.[30] observed a linear relationship between the log values of $T_B - T_F$ and E_a for relaxors with perovskite structures and the values obtained for the nonperovskite relaxor $AgNb_7O_{18}$ closely fit this linear trend. This relaxor behavior is not consistent with the unit cells having the centrosymmetric space group *Immm*; neither is it consistent with the chiral, nonpolar space groups *I*222 or $I2_12_12_1$. Instead it indicates that, locally, the room temperature structure is one of the three crystallographically distinct *Imm*2 variants (*I*2*mm*, *Im*2*m*, or *Imm*2) derived from the *Immm* parent structure.

Electron Diffraction. Selected area electron diffraction patterns (SADPs) were obtained from a number of zone axes. All were found to match simulations created using the $NaNb_7O_{18}$ structure determined by Marinder and Sundberg[18] (Figure 4).

The simulated patterns provide a good match to the SADPs obtained from $AgNb_7O_{18}$. These are consistent with the space group *Immm*, but cannot be used to distinguish between the alternative space groups under consideration as they all produce reflections in the same locations. In order to identify the space group, use has been made of a new convergent-beam diffraction technique. D-LACBED involves digitally combining separate convergent-beam diffraction patterns from individual sets of diffracting planes over a large range of beam tilts obtained from an area with a diameter of ~15 nm full width at half-maximum (fwhm).[21] The recombined diffraction patterns show the symmetry of the diffracted intensity from individual sets of planes with far greater clarity than can be obtained with the standard convergent-beam technique. The symmetry of the resultant diffraction group is related to the crystal point group, and the techniques set out by Buxton et al.[33] are used to determine the point groups that can give rise to the diffraction symmetry.

The bright field (BF) pattern in the center has both vertical and horizontal mirror planes, giving it symmetry 2mm. The whole pattern has a vertical mirror plane but not a horizontal mirror plane, shown most clearly by comparing the $\pm 0\,10\,0$ patterns. Opposing dark field patterns with $\pm\mathbf{g}$ vectors (e.g., $\bar{3}50$ and 350) are not equivalent when translated onto each other, demonstrating that the crystal structure is non-

dx.doi.org/10.1021/ic5007346 | Inorg. Chem. 2014, 53, 8941–8948

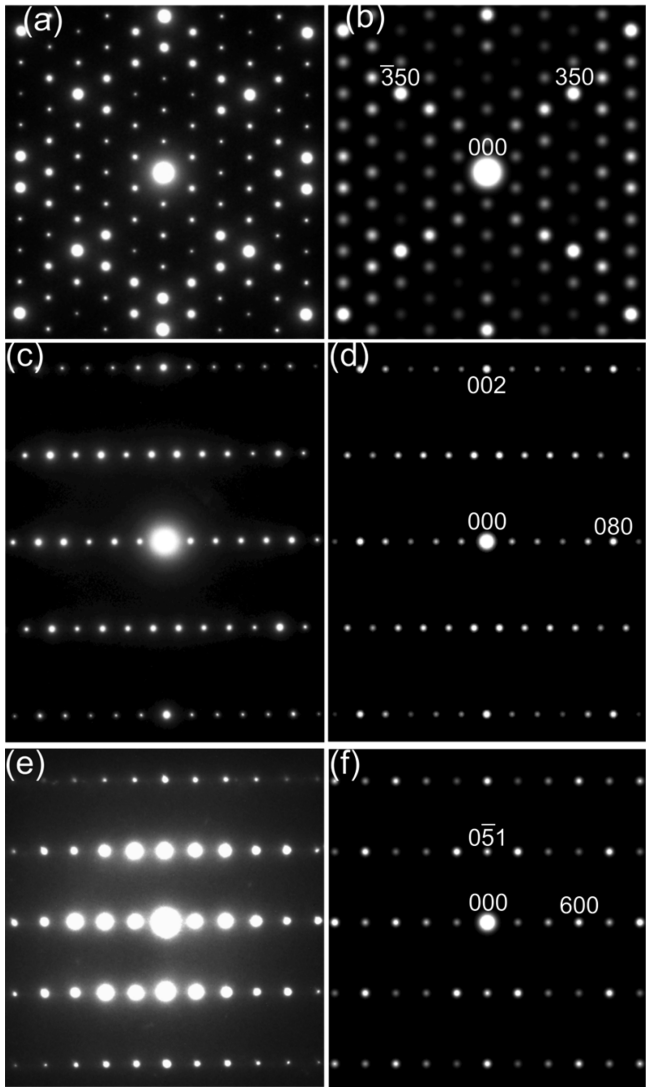

Figure 4. SADPs matched with simulations for $AgNb_7O_{18}$ from zone axes (a and b) [001], (c and d) [100], and (e and f) [015]. The simulated patterns are indexed.

centrosymmetric, at least on the scale of the electron beam. The projection diffraction group of the pattern is therefore $m1_R$. The absence of higher-order Laue zones (HOLZ) from this zone axis means that this projection diffraction group may possibly result from m or m_R diffraction groups as well. However, this pattern has been obtained from a ⟨100⟩ zone axis of an orthorhombic crystal, which can only correspond to point group $mm2$,[33] as predicted from the permittivity data. The absence of a horizontal mirror plane in Figure 5 indicates that there is no mirror plane perpendicular to the y direction, making it the polar axis. The space group must therefore be $Im2m$ in the configuration used by Marinder and Sundberg.[18] The $Im2m$ structure has the same shape and size as the $Immm$ structure, but the absence of the mirror plane perpendicular to y allows cation displacements along $\pm y$, leading to local breaking of the center of symmetry and the formation of two degenerate structures. A larger version of Figure 5, incorporating diffraction information from a far greater number of crystal planes, is in the Supporting Information.

X-ray Diffraction. Rietveld refinements were performed against XRD obtained from the powdered ceramic (Figure 6)

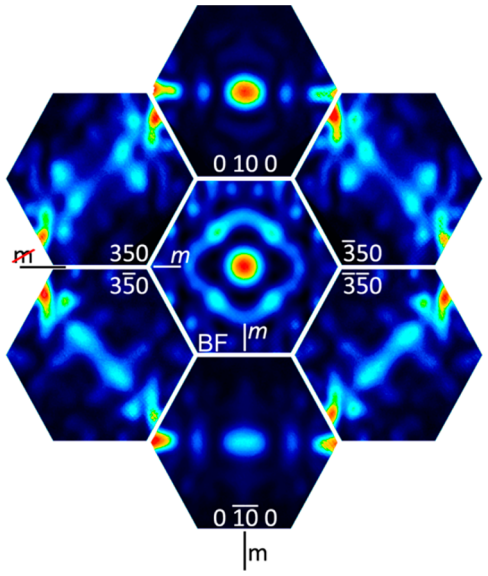

Figure 5. D-LACBED pattern obtained from [001] zone axis of $AgNb_7O_{18}$ (BF = bright field; m = mirror).

using the $NaNb_7O_{18}$ structure published by Marinder and Sundberg[18] as the initial model for a refinement in space group $Immm$. This model only accounted for half of the Ag^+ cations. In their paper, the authors stated that "several perovskite-type sites are available in the structure", referring to the cuboctahedral interstices similar to those where Ag^+ would normally be located in perovskite-structured materials. Ag^+ ions were added to these sites in the model and the occupancies were allowed to refine. Thermal parameters were refined with one value for each element. The thermal parameters of the five Nb^{5+} cations were subsequently allowed to take different values, but when this was extended to Ag^+ or O^{2-} species, several values fell below zero so the parameters were kept specific to the species, not the positions. The reflection profile was a Thompson−Cox−Hastings pseudo-Voigt function with an additional modification for anisotropic strain.[34] Once the refinement in space group $Immm$ was completed, the results were used to generate a model for the structure with space group $Im2m$. However, when refining this lower symmetry model, very little improvement in the fit parameters was observed and the uncertainty in the atomic coordinates became much larger. The results of the $Immm$ refinement are in Tables 1 and 2, and the results of the $Im2m$ refinement are in the Supporting Information.

Weak peaks at 22.6, 29.8, and 32.3° 2θ that are not accounted for by the model correspond closely to strong reflections expected from $AgNb_3O_8$.[9] The proportion of $AgNb_3O_8$ refines to less than 3% of the total volume.

The collected results require careful interpretation to resolve the discrepancy between the different symmetries observed by X-ray and electron diffraction. In a relaxor in the ergodic state, the polar axis of the unit cell does not have long-range correlation across the sample. However, XRD has a long correlation length and is collected from a large sample with grains of size ∼1 μm over a period of many hours. It therefore perceives a time-averaged structure which is nonpolar, in common with relaxor materials such as the perovskite $PbMg_{1/3}Nb_{2/3}O_3$, where X-ray and neutron diffraction perceive no deviation from the cubic prototype even at temperatures below T_F; ∼400 K below T_B.[31,35]

dx.doi.org/10.1021/ic5007346 | Inorg. Chem. 2014, 53, 8941−8948

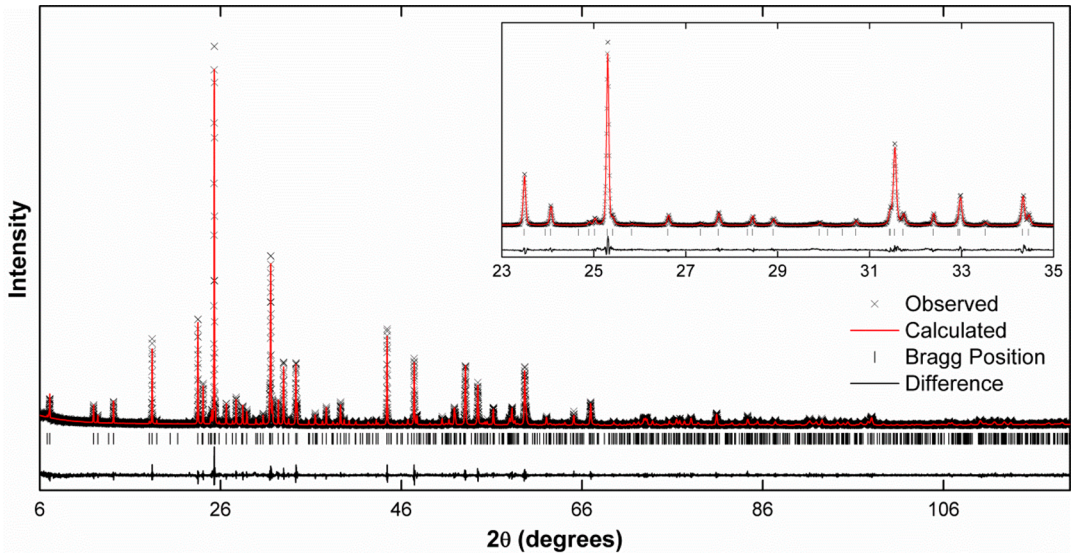

Figure 6. Full range of XRD data for $AgNb_7O_{18}$ with the calculated profile, positions of Bragg peaks, and the difference between the data plotted. The inset shows the data range that contains the three most intense peaks. The intensity is plotted on a linear scale.

Table 1. $AgNb_7O_{18}$ Refinement Parameters

crystal system	orthorhombic
space group	*Immm* (71)
a (Å)	14.33158(15)
b (Å)	26.15102(31)
c (Å)	3.83624(3)
V (Å^3)	1437.766(26)
density (g cm^{-3})	4.839(5)
refined parameters	68
R_{exp} (%)	19.859
R_p (%)	16.383
R_{wp} (%)	23.744
R_{Bragg} (%)	4.825
χ^2	1.196

As the PNRs are expected to be of the order of 10 nm, with rapid fluctuations in polarization direction,[36] electron diffraction from a relaxor material would normally be expected to also display nonpolar symmetry. However, it is important to consider that there will always be a distribution in PNR size, in which the largest regions fluctuate more slowly. Viehland et al.[24] showed that the frequency of the fluctuations depends very strongly on PNR size; their calculations show regions of size 45 and 55 Å with fluctuation frequencies that are different by 4 orders of magnitude. Moreover, several recent studies have shown that a significant fraction of PNRs are static in ergodic relaxors, far above T_F.[37−39] Although our electron diffraction information was collected from an area the size of the electron beam (∼15 nm diameter fwhm), this was located within a large region that was free from defects. We conclude that the frequency of polarization fluctuation in this region was

Table 2. Unit Cell Contents of $AgNb_7O_{18}$, Refined in Space Group *Immm*

atomic site	site sym	*x*	*y*	*z*	fractional occupation	U_{iso} (Å^2)
Ag1	2a	0	0	0	0.946(7)	0.0169(17)
Ag2	2b	1/2	0	0	0.320(6)	0.0169(17)
Ag3	8n	0.3075(13)	0.1053(9)	0	0.120(3)	0.0169(17)
Ag4	4h	0	0.2872(10)	0.5	0.139(5)	0.0169(17)
Nb1	8n	0.11970(17)	0.10269(12)	0.5	1	0.0020(8)
Nb2	8n	0.30630(21)	0.20720(12)	0.5	1	0.0037(9)
Nb3	4f	0.31413(31)	0	0.5	1	0.0141(15)
Nb4	4g	0	0.18972(16)	0	1	0.0022(11)
Nb5	4g	0	0.39491(19)	0	1	0.0128(12)
O1	8n	0.7005(11)	0.5550(7)	0	1	0.0080(13)
O2	8n	0.9027(11)	0.5577(7)	0	1	0.0080(13)
O3	8n	0.7104(11)	0.6598(6)	0	1	0.0080(13)
O4	8n	0.9050(11)	0.6616(6)	0	1	0.0080(13)
O5	8n	0.9020(10)	0.7666(6)	0	1	0.0080(13)
O6	8n	0.1006(10)	0.1192(6)	0	1	0.0080(13)
O7	8n	0.2924(11)	0.2237(7)	0	1	0.0080(13)
O8	4h	0	0.0640(9)	0.5	1	0.0080(13)
O9	4h	0	0.1627(9)	0.5	1	0.0080(13)
O10	4h	0	0.3887(10)	0.5	1	0.0080(13)
O11	4e	0.3037(16)	0	0	1	0.0080(13)

dx.doi.org/10.1021/ic5007346 | *Inorg. Chem.* 2014, 53, 8941−8948

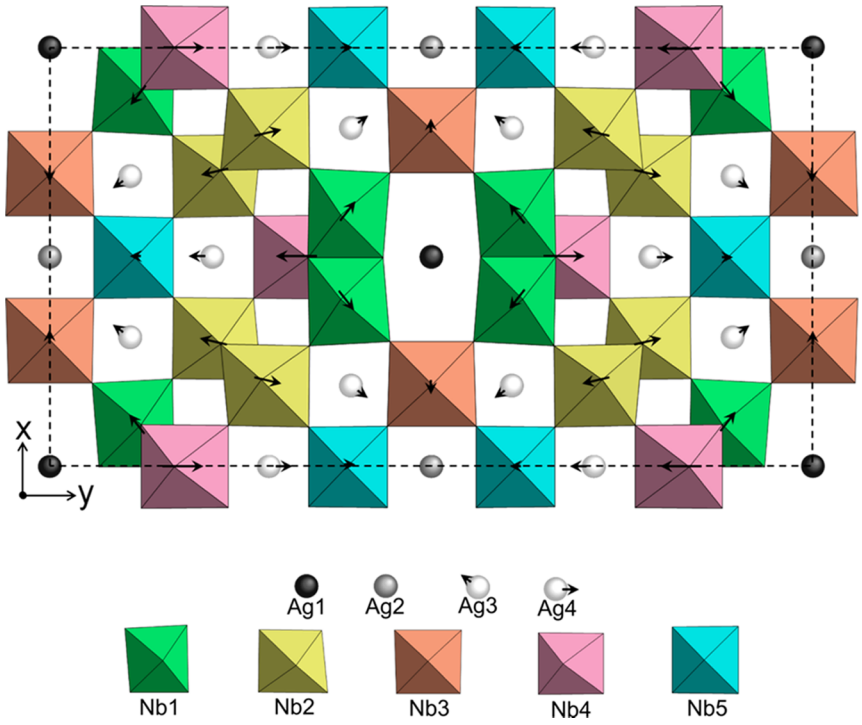

Figure 7. Refined $AgNb_7O_{18}$ unit cell, depicted as a network of NbO_6 octahedra. The unit cell is indicated by the dashed border. Colors indicate the NbO_6 octahedra that are related by symmetry. Arrows on octahedra indicate the direction and relative magnitude of the Nb^{5+} displacements from ideal locations. Labels for Ag atoms and NbO_6 octahedra correspond to their numbering scheme in Table 1. The darkness of the Ag^+ cations indicates the occupation of those sites (light = lowest occupation; dark = greatest occupation), and arrows next to Ag^+ cations indicate the direction and relative magnitude of their displacements from ideal (undistorted) locations. In order for cation displacements to be clear in the figure, they have been exaggerated by a factor of approximately 2.

sufficiently slow that the D-LACBED technique perceived a structure that retained some polar character.

The $AgNb_7O_{18}$ unit cell derived from the high-symmetry refinement is depicted in Figure 7. To a first approximation, the unit cell has the dimensions $5a_c/\sqrt{2} \times 9a_c/\sqrt{2} \times a_c$, where a_c is the lattice parameter of a pseudocubic perovskite unit cell. The refined lattice parameters give this unit cell the dimensions 4.05 Å × 4.11 Å × 3.84 Å, indicating that the octahedra are slightly extended along the polar direction and significantly compressed parallel to the *c* direction. The building block defined by the corner-shared NbO_6 octahedra and resembling the perovskite structure is depicted in Figure 8.

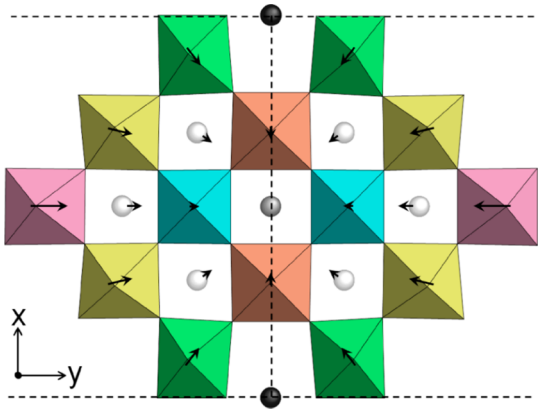

Figure 8. "Perovskite-like" building block of $AgNb_7O_{18}$. See Figure 7 caption for explanation of details.

Rietveld refinement has been used to establish the locations of the Ag^+ cations for the first time. There are four distinct Ag^+ sites which, if they were all fully occupied, would yield a material with the formula $Ag_4Nb_7O_{18}$, clearly a problem for maintaining charge neutrality. However, the occupancies of the Ag sites were refined to give a material with the empirical formula $Ag_{1.012(18)}Nb_7O_{18}$. This confirms that no significant quantities of Ag volatilized during synthesis and that Ag is present as Ag^+. The refined occupancies show that the Ag^+ has a strong preference for the largest interstice in the structure—the rectangular tunnel located at the center and corners of the unit cell—and a weaker preference for the cuboctahedral "perovskite-like sites". It has long been noted that relaxor behavior in perovskites and tungsten bronzes is associated with mixed species sharing a single crystallographic site, resulting in local heterogeneity (e.g., Viehland et al.[24]). In $AgNb_7O_{18}$, the heterogeneity is introduced by the partial occupation of the Ag sites.

In order to clarify and interpret the cation displacements in the structure, their magnitudes and directions have been calculated relative to both their "ideal" positions and the centers of the oxygen octahedra. Ideal positions are found by placing atoms on the nodes of a grid with the same dimensions as the unit cell, where *a* is divided into 10 parts, *b* is divided into 18 parts, and *c* is divided into 2 parts of equal length. The data are given in Table 3, and the cation displacements from the ideal positions can be seen in Figures 7 and 8.

Figure 8 shows that the structure of $AgNb_7O_{18}$ can be viewed as columns of perovskite-like material connected together by edge-sharing of the peripheral octahedra, which experience significant distortion. Statistically, in each layer of each column,

dx.doi.org/10.1021/ic5007346 | Inorg. Chem. 2014, 53, 8941−8948

Table 3. Cation-Related Data Obtained from Structural Refinement

cation	displacement from ideal position (Å)	direction of displacement (clockwise)	displacement from oxygen polyhedron center (Å)	direction of displacement (clockwise)
Ag1	0	–	0	–
Ag2	0	–	0	–
Ag3	0.186(22)	−54.4(2)° from [100]	0.144(23)	−62.0(3)° from [100]
Ag4	0.246(24)	[010]	0.119(27)	[010]
Nb1	0.358(3)	−37.954(2)° from [100]	0.377(7)	−47.67(2)° from [100]
Nb2	0.403(3)	−77.06(2)° from [100]	0.306(8)	−77.36(10)° from [100]
Nb3	0.203(4)	[100]	0.170(9)	[100]
Nb4	0.603(4)	[010]	0.469(9)	[010]
Nb5	0.157(5)	[010]	0.133(10)	[010]

one Ag^+ is located in one of the cuboctahedral sites, displaying a preference for the central site. The cation displacements are all directed toward the center of the perovskite-like unit, and the displacements increase in magnitude the further the cations are from the center of the unit. This indicates that the cations are being repelled from the edge-sharing zones, since if they were attracted to the center of the perovskite unit, the displacements would be largest for those cations closest to the center of the unit. Additionally, with the sole exception of Nb1, the displacements of all cations from their ideal positions are greater than their displacements from the center of their respective oxygen coordination polyhedra. This results from the oxygen framework moving away from the ideal position in the same direction as the cations. It is proposed that this repulsion is in mitigation of the locally high density in the edge-sharing zones. This suggests that the structure may experience high local stresses and indicates that this connectivity of octahedra is not particularly stable.

CONCLUSIONS

$AgNb_7O_{18}$ has been fabricated as dense ceramics without Ag loss. Permittivity data show a frequency-dependent response that is a classic indicator of a relaxor ferroelectric. Fitting the Volger−Fulcher equation to the data reveals an incipient transition to the nonergodic state, and high-temperature permittivity data indicate that the Burns temperature is ∼490 K. The local structure revealed by electron diffraction has the polar space group *Im*2*m*, but X-ray diffraction perceives a structure with the centrosymmetric space group *Immm*, apparently isomorphous with $NaNb_7O_{18}$. Rietveld refinements show that Ag^+ cations partially occupy all cuboctahedral sites but occupy the largest, rectangular sites almost completely. Both anions and cations appear to be repelled away from zones of edge-sharing octahedra.

ASSOCIATED CONTENT

Supporting Information

Crystallographic parameters for $AgNb_7O_{18}$ in CIF format. Complete D-LACBED data set (Figure S1) and results from Rietveld refinement in space group *Im*2*m* (Tables S1 and S2). This material is available free of charge via the Internet at http://pubs.acs.org.

AUTHOR INFORMATION

Corresponding Author

*E-mail: d.i.woodward@warwick.ac.uk.

Notes

The authors declare no competing financial interest.

ACKNOWLEDGMENTS

The PANalytical MPD diffractometer used in this research was obtained though the Science City Energy Futures Project: Hydrogen Energy, with support from Advantage West Midlands (AWM) and partly funded by the European Regional Development Fund (ERDF). R.B. was supported by EPSRC Grant EP/J009229/1. For crystallographic assistance and encouragement, it is a pleasure to thank Dean Keeble, Wook Jo, Antonio Feteira, and Ljuba Schmitt.

REFERENCES

(1) Mitchell, R. H. *Perovskites: Modern and Ancient*; Almaz Press Inc.: Thunder Bay, ON, Canada, 2002.
(2) Cava, R. J.; Krajewski, J. J.; Roth, R. S. *Mater. Res. Bull.* **1998**, *33*, 527−532.
(3) Lee, S.; Bock, J. A.; Trolier-McKinstry, S.; Randall, C. A. *J. Eur. Ceram. Soc.* **2012**, *32*, 3971−3988.
(4) Keeney, L.; Maity, T.; Schmidt, M.; Amann, A.; Deepak, N.; Petkov, N.; Roy, S.; Pemble, M. E.; Whatmore, R. W. *J. Am. Ceram. Soc.* **2013**, *96*, 2339−2357.
(5) Brusset, H.; Gillier-Pandraud, H.; Belle, J.-P. *Bull. Soc. Chim. Fr.* **1967**, *7*, 2276−2283.
(6) Yashima, M.; Matsuyama, S.; Sano, R.; Itoh, M.; Tsuda, K.; Fu, D. *Chem. Mater.* **2011**, *23*, 1643−1645.
(7) Woodward, D. I.; Thomas, P. A. *Appl. Phys. Lett.* **2011**, *98*, 132904.
(8) Masó, N.; Woodward, D. I.; Thomas, P. A.; Várez, A.; West, A. R. *J. Mater. Chem.* **2011**, *21*, 2715−2722.
(9) Rozier, P.; Szajwaj, O. *J. Solid State Chem.* **2008**, *181*, 228−234.
(10) Fu, D.; Endo, M.; Taniguchi, H.; Taniyama, T.; Koshihara, S.-Y.; Itoh, M. *Appl. Phys. Lett.* **2008**, *92*, 172905.
(11) Lei, C.; Ye, Z.-G. *J. Phys.: Condens. Matter* **2008**, *20*, 232201.
(12) Kato, H.; Kobayashi, H.; Kudo, A. *J. Phys. Chem. B* **2002**, *106*, 12441−12447.
(13) Palasyuk, O.; Maggard, P. A. *J. Solid State Chem.* **2012**, *191*, 263−270.
(14) Audier, M.; Chenevier, B.; Roussel, H.; Vincent, L.; Peña, A.; Lintanf Salaün, A. *J. Solid State Chem.* **2011**, *184*, 2033−2040.
(15) Le Gallic, M.; Roussel, H. *J. Solid State Chem.* **2013**, *200*, 143−149.
(16) Stennett, M. C.; Reaney, I. M.; Miles, G. C.; Woodward, D. I.; West, A. R.; Kirk, C. A.; Levin, I. *J. Appl. Phys.* **2007**, *101*, 104114.
(17) Lee, S.; Wilke, R. H. T.; Trolier-McKinstry, S.; Zhang, S.; Randall, C. A. *Appl. Phys. Lett.* **2010**, *96*, 031910.
(18) Marinder, B.-O.; Sundberg, M. *Acta Crystallogr., Sect. B* **1984**, *40*, 82−86.
(19) Cohen, R. E.; Krakauer, K. *Ferroelectrics* **1992**, *136*, 65−84.
(20) Hill, N. A. *J. Phys. Chem. B* **2000**, *104*, 6694−6709.
(21) Beanland, R.; Thomas, P.; Woodward, D. I.; Thomas, P. A.; Roemer, R. *Acta Crystallogr., Sect. A* **2013**, *69*, 427−434.
(22) Masó, N.; West, A. R. *J. Mater. Chem.* **2010**, *20*, 2082−2084.
(23) Cross, L. E. *Ferroelectrics* **1987**, *76*, 241.

(24) Viehland, D.; Jang, S. J.; Cross, L. E.; Wuttig, M. *J. Appl. Phys.* **1990**, *68*, 2916−2912.
(25) Bokov, A. A.; Ye, Z.-G. *J. Mater. Sci.* **2006**, *41*, 31−52.
(26) Tagantsev, A. K. *Phys. Rev. Lett.* **1994**, *72*, 1100−1103.
(27) Zhu, X. L.; Wu, S. Y.; Chen, X. M. *Appl. Phys. Lett.* **2007**, *91*, 162906.
(28) Ferrarelli, M. C.; Nuzhnyy, D.; Sinclair, D. C.; Kamba, S. *Phys. Rev. B* **2010**, *81*, 224112.
(29) Palasyuk, O.; Palasyuk, A.; Maggard, P. A. *Inorg. Chem.* **2010**, *49*, 10571−10578.
(30) Stringer, C. J.; Shrout, T. R.; Randall, C. A. *J. Appl. Phys.* **2007**, *101*, 054107.
(31) Burns, G.; Dacol, F. H. *Solid State Commun.* **1983**, *48*, 853−856.
(32) Viehland, D.; Jang, S. J.; Cross, L. E.; Wuttig, M. *Phys. Rev. B* **1992**, *46*, 8003−8006.
(33) Buxton, B. F.; Eades, J. A.; Steeds, J. W.; Rackham, G. M. *Philos. Trans. R. Soc., A* **1976**, *281*, 171−194.
(34) Stephens, P. W. *J. Appl. Crystallogr.* **1999**, *32*, 281−289.
(35) Bonneau, P.; Garnier, P.; Calvavrin, G.; Husson, E.; Gavarri, J. R.; Hewat, A. W.; Morell, A. *J. Solid State Chem.* **1991**, *91*, 350−361.
(36) Bokov, A. A.; Ye, Z.-G. *J. Adv. Dielectr.* **2012**, *2*, 1241010.
(37) Bokov, A. A.; Rodriguez, B. J.; Zhao, X.; Ko, J.-H.; Jesse, S.; Long, X.; Qu, W.; Kim, T. H.; Budai, J. D.; Morozovska, A. N.; Kojima, S.; Tan, X.; Kalinin, S. V.; Ye, Z.-G. *Z. Kristallogr.* **2011**, *226*, 99−107.
(38) Kholkin, A.; Morozovska, A. N.; Kiselev, D.; Bdikin, I.; Rodriguez, B. J.; Wu, P.; Bokov, A.; Ye, Z.-G.; Dkhil, B.; Chen, L.-Q.; Kosec, M.; Kalinin, S. V. *Adv. Funct. Mater.* **2011**, *21*, 1977−1987.
(39) Xie, L.; Li, Y. L.; Yu, R.; Cheng, Z. Y.; Wei, X. Y.; Yao, X.; Jia, C. L.; Urban, K.; Bokov, A. A.; Ye, Z.-G.; Zhu, J. *Phys. Rev. B* **2012**, *85*, 014118.